MultiResp: Robust Respiration Monitoring for Multiple Users using Acoustic Signal

Tianben Wang, Zhangben Li, Xiantao Liu, Tao Gu, *Senior Member, IEEE,* HongHao Yan, Jing Lv, Jin Hu, Daqing Zhang, *Fellow, IEEE*

Abstract—In recent years, we have seen efforts made to monitor respiration for multiple users. Existing approaches capture chest movement relying on signals directly reflected from chest or separate breath waves based on breath rate difference between subjects. However, several limitations exist: 1) they may fail when subjects face away from the transceiver or are blocked by obstacles or other subjects; 2) they may fail to separate subjects' breath waves with the same or similar rates (i.e., breath rate difference < 1 bpm); 3) they assume a priori knowledge of number of subjects and cannot adapt to dynamic change of subject number during monitoring. To overcome these limitations, in this paper we propose *MultiResp*, a multi-user respiration monitoring system using acoustic signal. By fully leveraging the abundant acoustic signals reflected indirectly from subjects' chest, *MultiResp* can robustly capture chest movement even when they face away from the transceiver or are blocked. By extracting fine-grained breath rate and phase difference between different subjects, *MultiResp* can separate the breath waves with the same or similar rates and adapt to dynamic change of subject number during monitoring. Extensive experiments show that *MultiResp* is able to accurately monitor the respiration of multiple users with a median error of 0.3 bpm in various indoor scenarios, however, it fails when the sound pressure is lower than 55 dB or body movement is happening.

Index Terms— Multi-user respiration monitoring, Acoustic sensing, Multipath reflection

1 Introduction

RESPIRATION monitoring plays a crucial role in diagnosing diseases such as chronic obstructive pulmonary disease (COPD)[1], heart failure[2], and sleep Apnea[3]. Monitoring respiration in clinical settings requires dedicated devices such as thoracic impedance pneumography [4], capnography [5] or pulse oximeter [6] which produce highly accurate results but may cause discomfort and even affect the underlying physiological parameters being measured [7]. In addition, these devices are costly and usually operated by well-trained professionals. Respiration monitoring in home settings include a range of devices and sensors such as wearable devices [8,9], smart mattress, smart pillow embedded with air pressure sensors [10], fiber optic sensor [11,12] and camera-based systems [13]. However, they can be still costly [10-12], may require long-time wearing [8,9] and raise privacy concerns [13].

Contactless respiration monitoring typically relies on RF or ultrasonic signals. Many approaches have been proposed, including RFID [14-17], Doppler radar [18-20], UWB radar [21-24], FMCW radar [25], WiFi [26-39] and acoustic devices [40-45], however these systems focus on single user only. Recent efforts have been made to enable multi-user respiration monitoring, e.g., FMCW radar [46-48], UWB radar [49], WiFi [50-54], Lora [55] and acoustic devices [56]. However, several limitations exist: 1) Existing systems rely on signals directly reflected from subjects' chests, thus they may not work when subjects face away from the transceiver, or they are blocked by furniture or other subjects. 2) They may not be able to separate breath waves with the same or similar rates (i.e., breath rate difference smaller than 1 bpm). 3) Existing systems assume priori knowledge of number of subjects and cannot adapt to dynamic change during monitoring. These limitations make existing systems impractical for real-world deployment.

To address the aforementioned limitations, in this paper, we present *MultiResp*, an acoustic based respiration monitoring system for multiple users. Our preliminary experiments show that when subjects breathe with different rates, the multipath signals belonging to the same subject vary with the same frequency (i.e., the subject's breath rate) and similar phases, while the multipath signals belonging to different subjects vary with different frequencies. When subjects breathe with the same rate but different phases, the multipath signals belonging to the same subject vary with the same frequency and similar phases, while the multipath signals belonging to different subjects vary with

- *T. Wang, Z. Li, X. Liu, H. Yan, J. Hu are with the College of Mechanical and Electronic Engineering, Northwest A&F University, Yangling 712100, China and Key Laboratory of Agricultural Internet of Things, Ministry of Agriculture and Rural Affairs, Yangling, 712100, China; E-mail: wangtb@nwafu.edu.cn; lzb996@nwafu.edu.cn, liuxt@nwafu.edu.cn; yanhonghao9@163.com; hujin007@nwsuaf.edu.cn.*
- *T. Gu is with the School of Computing at Macquarie University, Australia. E-mail: tao.gu@mq.edu.au.*
- *J. Lv is with the Department of Network&Education Technology Center, Northwest A&F University, Yangling 712100, China, E-mail: lvjing@nwafu.edu.cn.*
- *D. Zhang are with the School of Computer Science, Peking University, Beijing, China and Telecom SudParis, Institut Polytechnique de Paris, Évry Cedex, France. E-mail: dqzhang@sict.pku.edu.cn.*

xxxx-xxxx/0x/$xx.00 © 200x IEEE Published by the IEEE Computer Society

the same frequency but different phases. Driven by this observation, we firstly extract all multipath signals reflected from subjects' chests. We then group multipath signals corresponding to chest movement by frequency. Multipath signals in the same group are further grouped by phase. In this way, we can exactly obtain the multipath signal group corresponding to each subject even when subjects breathe with the same or similar rates, and the number of groups is exactly the number of subjects. However, this is not a trivial task due to several challenges:

1) When subjects face away from the transceiver or are blocked, there is no signal reflected directly from subjects' chests. We may use indirectly reflected signals, however, due to multipath effect and relatively long propagation distance, indirectly reflected signals can be very weak.

2) To address the limitation that existing systems fail to separate breath waves with the similar rates, we can measure the frequency of multipath signals, then group them by frequency. However, existing frequency measuring methods, e.g., fast Fourier transform (FFT), may not work effectively due to limited frequency resolution.

3) When subjects breathe with the same rate, we may group multipath signals by phase to separate breath waves. However, the phase derived from the phase spectrum is heavily distorted due to ambient and hardware noise.

To address these challenges, we first quantify multipath signals with channel impulse response (CIR) and globally search multipath signals with obvious periodicity. This method retains both directly and indirectly reflected signals. Thus, when directly reflected signal is not presented, we can use indirectly reflected signals. In this way, we improve system robustness when subjects face away from transceiver or are blocked. To tackle the second challenge, we propose a frequency measuring method to effectively group multipath signals by frequency. For the third challenge, we compute correlation coefficient to obtain pairwise phase differences rather than absolute phase information. We then further group multipath signals with the same frequency by phase.

We develop a prototype system and evaluate *MultiResp* in various indoor scenarios: 1) subjects face away from the transceiver or are blocked by furniture or other subjects; 2) subjects breathe with the similar rates; 3) subjects breathe with the same rate; 4) the number of subjects changes dynamically. Results demonstrate that *MultiResp* can simultaneously track the respiration of multiple users in various scenarios. However, it fails when the sound pressure is lower than 55 dB or body movement is happening. The demo video of *MultiResp* is available at https://tinyurl.com/2p9c93v3 and https://youtu.be/naB3rFrNSfE.

The main contributions of this paper can be summarized as follows:

1) We propose a novel human respiration extraction method leveraging on both directly and indirectly reflected acoustic signals to reliably monitor chest movement of multiple users. This method fills the gap in existing systems when directly reflected signals are not presented.

2) We propose a novel breath wave separation method to separate breath waves with the same or similar rates. More importantly, it can adapt to scenarios where the number of subjects changes dynamically.

3) We implement and evaluate *MultiResp* through extensive experiments in various indoor scenarios. Results demonstrate that *MultiResp* is able to robustly measure respiration for multiple users.

2 Related Work

2.1 RF-based Approach

2.1.1 Single-user Scenario

RFID [14-17], UWB radar [21-24], FMCW radar [25], Doppler radar [18-20] have been used in monitoring respiration. Comparing with these systems, commodity WiFi devices are cost-effective and widely available in home settings. Ubibreathe [26], WiBreathe [27] and Breathfinding [28] monitor respiration leveraging the amplitude change of WiFi Received Signal Strength Indicator (RSSI). Wi-Sleep [19] extracts WiFi channel state information (CSI) for respiration monitor. This system has been further improved by considering sleep posture and abnormal respiration [32]. Wang et al. [35] propose Fresnel zone theory to study WiFi sensing limitations. FullBreath [38], FarSense [57] and Fresnel Diffraction Model [39] improve the robustness of respiration monitoring through overlapped Fresnel zones, CSI ratio between multiple receiving antennas and WiFi diffraction phenomenon, respectively. However, these RF based approaches cannot be directly applied in a multi-user scenario and they rely on directly reflected signals.

2.1.2 Multi-user Scenario

CW radar [58], UWB radar [49], and millimeter-wave radar [59] have been applied for multi-user respiration monitoring. Adib et al. [46] and Ahmad et al. [47] use FMCW radar to track multi-user respiration by simultaneously estimate the distance from chest to transceiver. DeepBreath [48] firstly transforms multi-user breath wave separation to a Blind Source Separation problem and solve it with the Independent Component Analysis (ICA) algorithm. It is able to separate breath waves with very different rates, but the number of subjects has to be known in advance, and it does not work when subjects breathe with similar rates. Zhang et al. [55] search and extract breath rate using Lora beamforming. Due to directional searching, this system fails if multiple subjects stay in the same direction. A popular RF based solution is to extract respiration rates from WiFi CSI. Liu et al. [34] firstly extract multi-user respiration rates from the power spectral density (PSD) of CSI amplitude. However, the Fresnel zone model demonstrates that CSI amplitude may have little variation at some locations. PhaseBeat [51] and TensorBeat [52] mitigate this problem leveraging on CSI phase. TR-BREATH [53] projects CSI to the Time-Reversal Resonating Strength (TRRS) feature space and extract subjects' respiration rate by the Root-MUSIC algorithm. MultiSense [54] tracks respiration by solving a blind source separation (BBS) problem with the ICA algorithm on CSI. The above systems rely on directly reflected signals and need priori knowledge of the number of subjects. It's hard for them to separate breath waves with very similar rates (breath rate difference < 1 bpm) and

same rate.

2.2 Audio-based Approach

2.2.1 Single-user Scenario

Acoustic signal has also been used to monitor respiration in recent years. Apneapp [40] measures breath rate and detects sleep Apnea by estimating the distance variation caused by chest movement during breathing with 18KHz~20KHz audio chirp signal. However, limited by its ranging resolution (7 mm), it may fail to measure chest displacement smaller than 1.4 cm. To improve range resolution, 240KHz ultrasonic is applied to measure chest movement in [41]. Although the system achieves accurate ranging, it requires costly ultrasonic transceiver. Wang et al. [42] propose a novel acoustic ranging method C-FMCW, which achieves a range resolution of around 0.4 cm on commodity acoustic device. Wang et al. [45] expand the frequency band of acoustic signal by transforming white noise into FMCW chirp and enhance SNR with mic array beamforming to achieve accurate respiration monitoring for infant. Xu et al. [60] propose a fine-grained breathing monitoring system by combining Energy Spectrum Density, Ensemble Empirical Mode Decomposition and Generative Adversarial Network in driving environments. In addition to measuring chest movement, directly sensing exhaled airflow is another way to monitor respiration. Arlotto et al. [43] propose minute Doppler shift caused by scattering effect of exhaled airflow on acoustic signal for respiration monitoring. The work [44] enhances the theory by building the model of the Doppler effect caused by exhaled airflow. Based on this model, it improves the robustness of respiration monitoring.

The above audio-based approaches are designed for single-user scenario. In addition, they rely on directly reflected signals, therefore fail to work when subjects face away from the transceiver or are blocked by furniture.

2.2.2 Multi-user Scenario

Wan et al. [56] propose the first multi-user respiration monitoring system using acoustic signals, named RespTracker, leveraging the distance derived from the time delay of reflected signals. However, there are several limitations remain to be addressed. Firstly, when subjects face away from the transceiver, there is no signal directly reflected from subject's chest. The time delays of indirectly reflected signals from the same subject are not gathering any more. The time delays of multipath signals belonging to different subjects may overlap heavily. In this case, it is difficult, to get accurate distance information. Secondly, RespTracker requires priori knowledge of number of subjects because the K-means cluster algorithm is used to separate multipath signals. Thirdly, it may fail to separate breath waves when subjects locate closely or breathe with very similar rates and same rate.

In contrast, we propose *MultiResp* to address the limitations of existing work by fully leveraging abundant acoustic signals indirectly reflected from subjects' chests, considering subject difference in terms of respiration rate and respiration phase.

3 System Overview

3.1 Motivation

To gain a clear understanding of design challenges, we firstly introuduce the concepts of CIR and CIR sequence, then conduct a preliminary experiment to provide further insight into these concepts.

With respect to CSI, CIR can describe both time delay and amplitude attenuation of each multipath reflection signal in time domain, hence avoiding the time-consuming signal decomposition process. With $x_t(n)$ and $x_r(n)$ (i.e., the echo received by microphone), CIR can be estimated using inverse filter [61]:

$$\hat{h}(n) = \mathrm{IFFT}\big(X_r(n) \times C(n)\big) \tag{1}$$

where $C(n)$ is the discrete Fourier transformation (DFT) of the inverse filter of $x_t(n)$. It is given by:

$$C(n) = \frac{{X_t}^*(n)}{{X_t}^*(n) \times X_t(n) + \varepsilon(n)} \tag{2}$$

IFFT denotes Inverse Fast Fourier transform. $X_r(n)$ and $X_t(n)$ are the DFT of $x_r(n)$ and $x_t(n)$, respectively. ${X_t}^*(n)$ is the conjugate of $X_t(n)$. $\varepsilon(n)$ is a small regularization parameter applied to avoid interference outside the frequency range of $x_t(n)$. Specifically, the value of $\varepsilon(n)$ should be very small within the frequency range of $x_t(n)$, while very large beyond the frequency range of $x_t(n)$. In other word, $\varepsilon(n)$ plays the role of a band stop filter.

Fig.1 shows an example of CIR estimated in a room. It describes the time delay and amplitude attenuation of all the multipath reflection signal, where each point denotes one signal path.

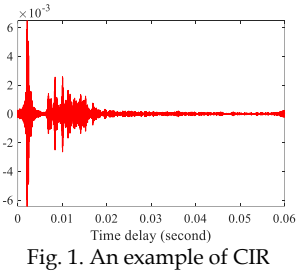

Fig. 1. An example of CIR

Let $\hat{h}_{t_i}(n)$ denote the CIR at time t_i, which describes the time delay and amplitude of all the multipath reflection signal at t_i. CIRs over time forms a matrix $\boldsymbol{S}$:

$$\boldsymbol{S} = \begin{bmatrix} \hat{\boldsymbol{h}}_{\boldsymbol{t_1}} \\ \hat{\boldsymbol{h}}_{\boldsymbol{t_2}} \\ \vdots \\ \hat{\boldsymbol{h}}_{\boldsymbol{t_N}} \end{bmatrix} = \begin{bmatrix} \hat{h}_{t_1}(1) & \hat{h}_{t_1}(2) & \cdots & \hat{h}_{t_1}(k) \\ \hat{h}_{t_2}(1) & \hat{h}_{t_2}(2) & \cdots & \hat{h}_{t_2}(k) \\ \vdots & \vdots & \vdots & \vdots \\ \hat{h}_{t_N}(1) & \hat{h}_{t_N}(2) & \cdots & \hat{h}_{t_N}(k) \end{bmatrix} = [\boldsymbol{S_1}, \boldsymbol{S_2}, \cdots, \boldsymbol{S_k}] \tag{3}$$

$\boldsymbol{S_i}$, $1 < i < k$, is the ith column of $\boldsymbol{S}$. It denotes the multipath signal with time delay i/f_s. For sake of simplicity, we call $\boldsymbol{S_i}$ one **CIR sequence**. In each iteration cycle of *MultiResp*, matrix $\boldsymbol{S}$ is updated. The CIR estimated in the current iteration cycle is added as a new row to the end of $\boldsymbol{S}$. If the number of the row is larger than 200 (the length of analysis window), i.e., the analysis window is overflowed, the first

row of $\boldsymbol{S}$ will be eliminated.

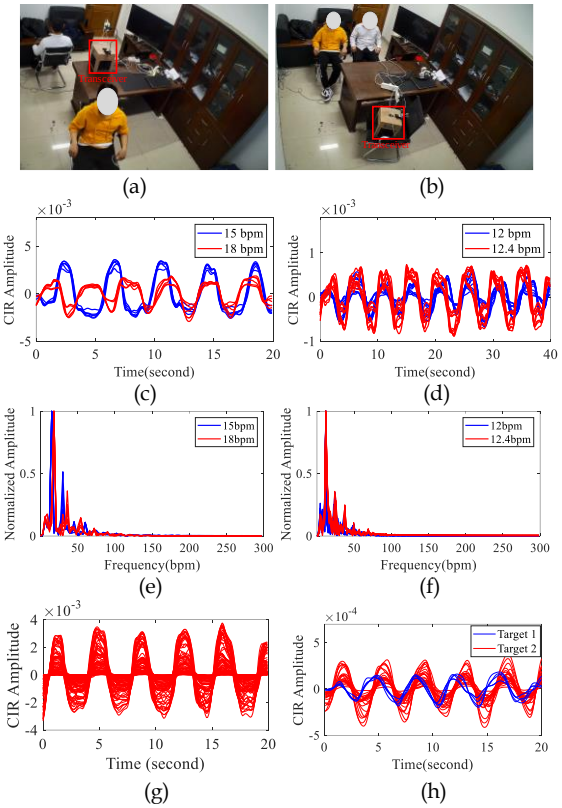

Fig. 2. Preliminary experiments

Fig. 2 shows the result from our preliminary experiment. As shown in Fig. 2(a), two subjects face away from the transceiver and breathe with 15 bpm and 18 bpm rates, respectively. Fig. 2(b) shows a scenario where two subjects sit closely and are blocked by a table. They breathe with 12 bpm and 12.5 bpm rates, respectively. Fig. 2(c) and Fig. 2(d) show the periodical CIR sequences obtained in the above two scenarios, respectively. Each line denotes one CIR sequence, which essentially presents the amplitude variation of one multipath signal. In general, there are more than one multipath signal reflected from subject's chest, so the number of the CIR sequences corresponding to each subject's respiration is larger than one. Because the chest movement during breathing is periodical, so the CIR sequences corresponding to subjects' chest movement show strong periodicity. We observe that the frequencies of the red and blue CIR sequence clusters are consistent with two subjects' breath rates, respectively. We know that in above scenarios there is no signal directly reflected from subjects' chests. So, these CIR sequences corresponding to breathing come from indirectly reflected signals only. It indicates that it is possible to take advantage of abundant multipath reflection, especially indirectly reflected signals, for better robustness. However, due to multiple reflection and relatively long propagation distance, indirectly reflected multipath signal can be very weak. So, the first question is how to extract indirectly reflected multipath signals in a reliable way.

Fig. 2(e) and Fig. 2(f) show the magnitude spectrum, calculated by FFT, of the CIR sequences in Fig. 2(c) and Fig. 2(d), respectively. We observe that FFT can distinguish the CIR sequences belonging to different subjects when subjects breathe with very different rates and fail when the subjects breathe with similar rates. Therefore, the second question to us is how to separate CIR sequences corresponding to different subjects, especially breathing with similar rates, in a robust manner.

Fig. 2(g) shows the periodical CIR sequences when a single subject is breathing. We observe that these CIR sequences have the same frequency and very similar phase. Fig. 2(h) shows the periodical CIR sequences when two subjects breathe with the same rate but different phases (i.e., the phase difference is about $\pi/4$). We observe that the CIR sequences belonging to the same subject show the same frequency and similar phase, while the CIR sequences belonging to different subjects show the same frequency but obviously different phases. It indicates that when subjects breathe with the same frequency, the CIR sequences can be separated using phase difference. However, from Fig. 2(g) and Fig. 2(h), we observe that the CIR sequences are mixed with irregular noise interference, i.e., the phase information is corrupted with non-negligible error. Hence, the third key question to us is how to accurately measure the phase of CIR sequences, and subsequently group them by phase.

3.2 System Design

We design *MultiResp* to address the aforementioned three questions, and Fig. 3 outlines the system framework.

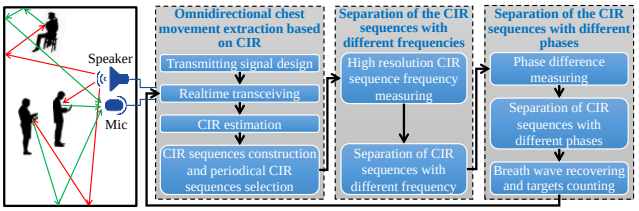

Fig. 3. System framework

Firstly, we use a speaker to contiously transmit a sinusoidal frequency modulated signal, and a microphone to receive reflected acoustic signals from the static environment and subjects synchronously. Based on transmitted and received signals, we estimate the CIR, which can quantify the time delay and attenuation of all multipath reflection signals. The CIRs over time form a matrix (each row is a CIR and each column we call it a CIR sequence), we extract the CIR sequences with high periodicity using autocorrelation function. The periodical CIR sequences correspond to subjects' chest movement during breathing. This is due to the fact that subjects' chest movement during breathing is periodical, so the reflection paths affected by subjects' chest movement varies periodical over time, while, the paths only reflected by the environment show no periodicity. The above method is essentially a global search method which ensures the robustness of chest movement information extraction in the extreme scenarios with no directly reflected multipath signals.

We then separate the periodical CIR sequences by frequency, i.e., breathing rate. Specifically, we propose a

high-resolution frequency measuring method, providing better frequency resolution than FFT. It is designed to distinguish 0.4 bpm breath rate difference with only 200 samples without zero padding. Based on this method, the CIR sequences can be grouped into different clusters by frequency. Within each cluster, the CIR sequences have the same frequency. For each cluster, we obtain pair-wise phase differences using correlation coefficient, which can mitigate noise interference. CIR sequences in the current cluster are then further grouped by the proposed two-stage clustering algorithm. Thus, we can exactly get the CIR sequence clusters corresponding to each subject. Finally, we recover the breath wave of each subject by merging the CIR sequences in each cluster. The above process is repeated to monitor subjects' respiration in real time.

4 Omnidirectional Chest Movement Extraction Based on CIR

We estimate CIR to quantify the acoustic multipath reflection, then extract chest movement information from CIRs over time by measuring the periodicity of CIR sequences.

4.1 Transmitting Signal Design and Transceiving Control

To estimate CIR, the transmitted signal should be designed with a wide frequency band. As *MultiResp* focuses on monitoring respiration during sleep, one of the key considerations when designing the transmit signal is audible noise. Traditional transmiting signals such as Training Sequence Code, Zadoff-Chu code, FMCW signal have an advantage in distance resolution due to zero autocorrelation characteristic or linear relationship between frequency difference and distance. However, even though they are modulated on a carrier whose frequency is higher than 20 kHz, they may still introduce audible noise in practice because of their discontinuous phase variation over time. In order to completely avoid the noise embedded in transmitting signal, the transmitting signal in *MultiResp* is designed as sinusoidal frequency modulated signal whose phase variation over time is smooth and continous. The frequency of the transmitted signal at time t is given by:

$$f(t) = f_c + \frac{B}{2}\left(1 + sin(2\pi t/T)\right), 0 \le t \le T \qquad (4)$$

where f_c, B and T denote carrier frequency, modulation bandwidth, and modulation period, respectively. To avoid audible noise, f_c should be higher than 18KHz. The phase is the integral of $f(t)$ over time,

$$u(t) = 2\pi \int_0^t f(t')dt' = 2\pi\left(f_c t + \frac{Bt}{2} - \frac{BT}{4\pi} cos\left(\frac{2\pi t}{T}\right)\right) \qquad (5)$$

Then, the transmitted signal can be presented as $x_t(t) = cos\big(u(t)\big)$. To meet the zero-state requirement (precondition before CIR estimation), $x_t(t)$ has to be modified as a pulse with a duty cycle. The discrete transmitted signal is finally represented as follows:

$$x_t(n) = \begin{cases} \cos\big(u(nT_s)\big)h(nT_s), & 0 \le nT_s \le T \\ 0 & T \le nT_s \le T' \end{cases} \qquad (6)$$

where $h(t)$ is a Hanning window, which is applied to mitigate spectrum leakage caused by sudden amplitude changes. $T_s = 1/f_s$ is the sampling interval. T' is the transmitting period, $T' > T$. To avoid echo overlap, $T' - T$ should be larger than multipath delay. Generally, a larger room has a larger multipath delay, thus requires a larger $T' - T$. Fig. 4 shows an example of a transmitted signal ($f_s = 96$KHz, $f_c = 26$KHz, $B = 2$KHz, $T = 0.04$s, $T' = 0.1$s).

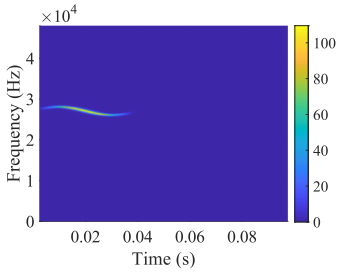

Fig. 4. The time-frequency spectrum of the transmitted signal

MultiResp controls the transceiver to continuously transmit the designed signal and receive echo frame. Specifically, the designed signal is continuously transmitted by the speaker in a non-blocking manner, meanwhile, the microphone receives the echo frame synchronously. Note that the length of the echo frame has to be the same as that of the transmitting signal.

With the transmitted signal and echo frame, we estimate CIR using Eq. (1). CIRs over time forms a matrix $\boldsymbol{S}$ shown in Eq. (2) and we get all CIR sequences as the columns of $\boldsymbol{S}$.

4.2 Periodical CIR Sequence Selection

4.2.1 CIR Sequence Variation Analysis

To facilitate the analysis, we consider single user scenario. As shown in Fig. 5 (a), if the subject directly faces the transceiver. Some of the multipath signals are always directly reflected from chests and finally received by transceiver. The CIR peaks corresponding to these multipath signals will move back and forth along the time delay axis [56]. However, the above example is an ideal scenario. In real scenarios, subjects may not directly face the transceiver. Under these conditions, the propagation routes of reflected signals can be roughly categorized into three types: 1) speaker → static environment ↔ chest → mic, 2) speaker → chest ↔ static environment →mic, 3) speaker → static environment ↔ chest ↔ static environment → mic, where double sided arrow denotes the possible reciprocating reflection. Due to multiple reflection, minute chest movement will amplify the change of reflection angle and finally result in multipath signal disappearing. As shown in Fig. 5(b), two multipath signals are indirectly reflected by chest and finally are received by transceiver at the end of exhaling. When starting inhaling, both two multipath signals disappear because reflection angle changes. The shape change of cloth wrinkle caused by chest movement further aggravates this phenomenon. This process appears as the synchronous appearance and disappearance of the

two CIR peaks, which correspond to the two multipath signals. The synchronous appearance and disappearance of the two CIR peaks will result in some of the CIR sequences vary periodically with the same frequency and similar phases. The CIR sequences shown in Fig. 2(g) demonstrates our analysis.

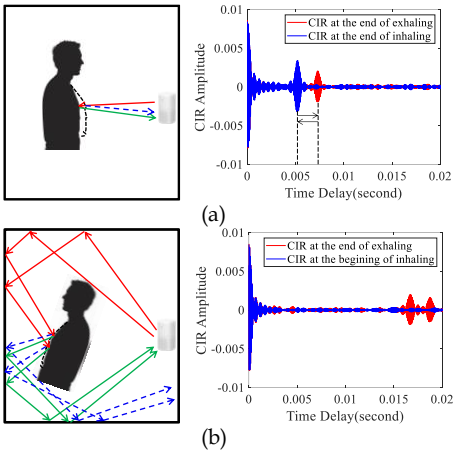

Fig. 5. Directly and indirectly reflected signals

Based on the above analysis, we can derive that:

1) If multiple subjects breathe with different rates, the CIR sequences belonging to same subject will vary with the same frequency as the breath rate of this subject. The CIR sequences belonging to different subjects will vary with different frequencies. The preliminary experiment results demonstrate this conclusion, as shown in Fig. 2(c) and Fig. 2(d).

2) If multiple subjects breathe with the same rate but different phases, the CIR sequences belonging to different subjects will vary with the same frequency but different phases. The preliminary experiment results demonstrate this conclusion, as shown in Fig. 2(h).

4.2.2 Periodical CIR Sequence Selection using Autocorrelation

Based on the above analysis, we know that regardless of targets breathing rate, the CIR sequences corresponding to targets' chest movement during breathing vary periodically. We obtain these periodical CIR sequences by measuring their periodicities. Specifically, we firstly remove polynomial trend embedded in CIR sequences using least-square regression. Then, we measure their autocorrelation. The autocorrelation of CIR sequence $\boldsymbol{S_i}$ is given by:

$$R_x(k) = \frac{c_k}{c_0} \tag{7}$$

where c_k is the auto-covariance of $\boldsymbol{S_i}$,

$$c_k = \frac{1}{N}\sum_{n=1}^{N-k}(\boldsymbol{S_i}(n) - \bar{\boldsymbol{S_i}})(\boldsymbol{S_i}(n+k) - \bar{\boldsymbol{S_i}}) \quad k = 0,1,\dots,N-1 \tag{8}$$

Fig. 6(a) shows two detrended CIR sequences. The red line has obvious periodicity, while the blue line is aperiodic. Fig. 6(b) shows their autocorrelations. We observe that the autocorrelation of the periodical sequence looks like a sinusoid, but amplitude decreases gradually, while the autocorrelation of the aperiodic sequence varies irregularly. It is easy to select all the periodical CIR sequences corresponding to respiration using the simple rule that a higher peak of the autocorrelation function means stronger periodicity.

Essentially, the above method is one of the global search methods. It extracts CIR sequences corresponding to chest movement. These CIR sequences selected by the method may be redundant for respiration monitoring in simple scenarios, for example, subjects face towards the transceiver, but it ensures the robustness of chest movement extraction when there is no directly reflected signals.

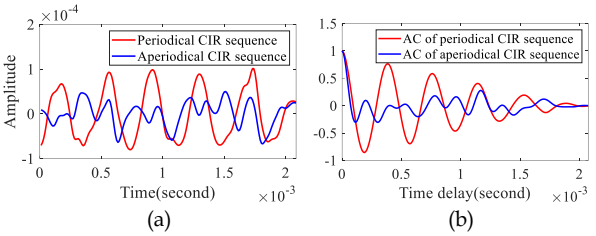

Fig. 6. Autocorrelation of CIR sequence

5 Separation of The CIR Sequences with Different Frequencies

Based on the preliminary experiments and the analysis in Section 4.3.1, we know that if multiple subjects breathe with different rates, the CIR sequences belonging to different subjects will vary with different frequencies. We separate the CIR sequences by accurately measuring their frequencies.

5.1 High Resolution CIR Sequence Frequency Measurement

Fast Fourier transform (FFT) is a classic tool for spectrum analysis. Its frequency resolution Δf is restrict by $\Delta f = f_s'/N$. f_s' and N denote the CIR estimation frequency and the length of CIR sequence, respectively. Generally, $f_s' = 10$ Hz is adequate for monitoring respiration signals that have typical frequency of 0.17 ~ 0.42 Hz, i.e., 10 bpm ~ 25 bpm. Considering the realtime performance, $N = 200$ (corresponding to the time window with $N/f_s' = 200/10 = 20$ seconds) is adequate. Thus, we can get the frequency resolution FFT as $\Delta f = f_s'/N = 10/200 = 0.05$ Hz $= 3$ bpm. In other words, the maximum respiration rate estimation error of FFT without zero padding is 3 bpm. It's well known that a larger N (including zero padding to N) results higher frequency resolution, with a higher cost in computation. Specifically, if the maximum of frequency resolution is set as 0.4 bpm (which is the highest frequency resolution of *MultiResp*. Please refer to Sec. 7.2.2.1), we have to zero pad periodical CIR sequence at least to the length $N = 1500$, thus the frequency resolution reaches $f_s'/N = 10/1500 = 0.0067$ Hz $= 0.4$ bpm. It's well known that FFT runs faster if the length of the signal is an integer power of 2. Thus, setting N as 2048 is adequate. In various application scenarios the number of selected periodical CIR sequence varies from about 50 to 800. Without loss of generality, we assume the average number of selected periodical CIR sequence is 425. Then FFT is performed on all periodical CIR

sequences, i.e., a 2048×425 matrix to get spectrum. This time comsuming process may significantly affect the realtime performance of *MultiResp*. We propose a method not only obtain the precise frequency of periodical CIR sequences but also significantly reduce the computation burden.

Fig. 7(a) shows two CIR sequences with frequencies 18 bpm and 19 bpm, respectively. Fig. 7(b) shows their magnitude spectrum calculated by FFT without zero padding. We can observe that the main frequencies estimated by FFT of both two CIR sequences are all 18 bpm. That is, FFT without zero padding can not distinguish 18 bmp and 19 bpm CIR sequences. We tackle this problem in time domain. Specifically, we compare time difference of the two CIR sequences accumulated over multiple periods. Let's consider the above instance again. The period length difference between 18 bpm CIR sequence and 19 bpm CIR sequence is $60/18 - 60/19 \approx 0.175$ s, which is slighter larger than sampling period $T' = 1/f_s' = 0.1$ s. To improve the robustness, rather than comparing single periods, we compare the length difference of multiple periods. Assuming the noise is additive white noise, time length difference of three periods is $3 \times (60/18 - 60/19) \approx 0.53$ s, which is much larger than sampling period and make it easily to distinguish 18 bpm and 19 bpm.

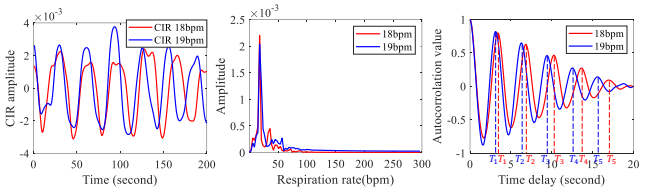

(a) (b) (c)

Fig. 7. Comparing the frequency resolution of FFT and our method

According to the definition of autocorrelation function, we know that the time delay of the nth peak of CIR sequence autocorrelation is exactly the time length of n periods, T_n, of CIR sequence. Fig. 7(c) shows the autocorrelations of the CIR sequences in Fig. 7(a). We get T_n of CIR sequence by finding the peaks of its autocorrelation. The relationship between breath rate R and T_n is:

$$T_n = \frac{60}{R} \times \frac{1}{T'} \times n \tag{9}$$

n periods time length difference between CIR sequences corresponding to breath rate R_1 and R_2 is:

$$\Delta T_n = \frac{60n(R_2 - R_1)}{R_1 R_2 T'} \tag{10}$$

A larger n means larger resolution. From Fig. 7(c), we see that as n increases, the time difference between T_n becomes more obvious. In practice, n should not be larger than the minimum number of the breaths contained in the time window. In our setting, time window length $N = 200$ (corresponding to $N/f_s' = 200/10 = 20$ seconds) contains at least 3 breaths. Thus, $n = 3$ is adequate. If breath rate is relatively high, T_4 and T_5 are better. Obviously, this method is built on the autocorrelation of periodical CIR sequences, which already have been obtained when selecting periodical CIR sequences (Sec. 4.3.2). It significantly reduces the computation burden.

5.2 CIR Sequences Separation based on Frequency

After obtaining T_3 of all the periodical CIR sequences, statistical analysis was performed. Fig. 8(a) shows all the periodical CIR sequences corresponding to the respiration of three subjects whose breath rates are 15 bpm, 19 bpm and 20 bpm, respectively. Each line denotes one CIR sequence. Fig. 8(b) shows the statistical histogram of T_3 of these CIR sequences. We observe that the histogram shows three distinct peaks who exactly correspond to respiration rates of three subjects. Only the CIR sequences whose T_3 value is neighboring to the peaks are reserved. In this setting, the CIR sequences whose T_3 value is within $[T_3^{p_i} - 0.1, T_3^{p_i} + 0.1]$ ($T_3^{p_i}$ denotes the T_3 value of the ith peak in histogram) are reserved. Thus, the CIR sequences corresponding to different frequency respiration are separated. Fig. 8(c) shows CIR sequences corresponding to the respiration with 20 bpm. We observe that some of the CIR sequences have opposite phases, i.e., their phase difference is π. Directly adding them to form breath wave will lead to cancelling each other out. For CIR sequences $\boldsymbol{S_{k_1}}, \boldsymbol{S_{k_2}}, \ldots$, belonging to the same frequency respiration, if $\|\boldsymbol{S_{k_1}} + \boldsymbol{S_{k_i}}\|_1 < \|\boldsymbol{S_{k_1}} - \boldsymbol{S_{k_i}}\|_1$, $\boldsymbol{S_{k_i}}$ is flipped along the time axis. Fig. 8(d) shows the synchronized CIR sequences corresponding to the respiration with 20 bpm.

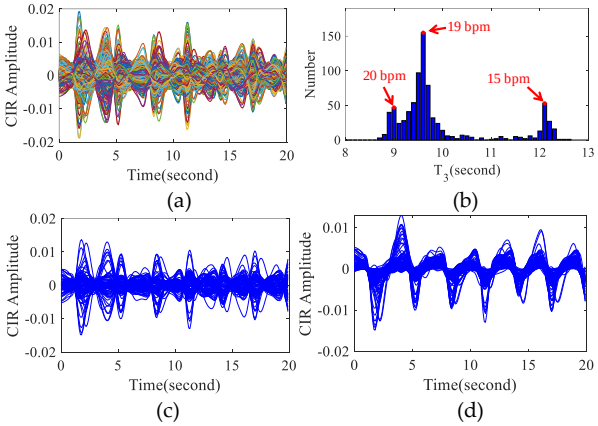

(a) (b) (c) (d)

Fig. 8. CIR sequences frequency measuring and classification

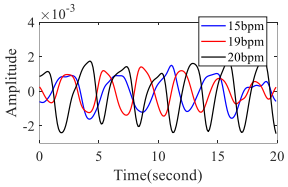

Fig. 9. Recovered breath waves with different frequencies

If all the subjects breathe with different frequencies, breath waves can be directly recovered as the average of the synchronized CIR sequence cluster. Fig. 9 shows the recovered breath waves of the three subjects who breathe with 15 bpm, 19 bpm and 20 bpm rates, respectively. In summary, the method described in this section is able to separate the breath waves with different frequencies without knowing the number of subjects in advance.

6 Separation of The CIR Sequences with Different Phases

6.1 Phase Difference Measurement

As shown in Fig. 8(d), due to the influence of ambient noise and hardware noise, CIR sequences corresponding to respiration contain random fluctuations. Directly extracting phase from phase spectrum will introduce non-negligible phase error. We use correlation coefficient (CC) to measure the phase difference between each pair of CIR sequences with the same frequency. Suppose the set of CIR sequences with the same frequency is $\boldsymbol{S}' = [\boldsymbol{S}_{k_1}, \boldsymbol{S}_{k_2}, \dots, \boldsymbol{S}_{k_M}]$, the CC matrix of $\boldsymbol{S}'$ is defined as:

$$\boldsymbol{R} = \begin{bmatrix} \rho_{11} & \rho_{12} & \cdots & \rho_{1M} \\ \rho_{21} & \rho_{22} & \cdots & \rho_{2M} \\ \vdots & \vdots & \ddots & \vdots \\ \rho_{M1} & \rho_{M2} & \cdots & \rho_{MM} \end{bmatrix} \tag{11}$$

where $\rho_{ij}, 1 \le i, j \le M$ denotes the CC between $\boldsymbol{S}_{k_i}$ and $\boldsymbol{S}_{k_j}$. CC can shield amplitude difference between a pair of CIR sequences and only reflect their phase difference. Smaller phase difference results in larger CC.

6.2 Two-stage CIR Sequences Clustering based on Phase Difference

In the first clustering stage, the algorithm finds and groups the CIR sequences corresponding to the same body part of one subject's chest. In the second stage, the algorithm merges the clusters corresponding to different part of chest of the same subject.

6.2.1 First-stage Clustering

The first-stage clustering algorithm operates on CC matrix to find all CIR sequence clusters corresponding to the same body part of one subject's chest. Because the variations of the CIR sequences corresponding to the same body part of one subject's chest are very similar, our idea is to find all compact CIR sequence clusters. Algorithm 1 shows the detailed clustering process.

Algorithm 1: *First stage CIR sequence clustering algorithm*

Input: CC matrix $\boldsymbol{R}$ of the CIR sequences with same freuquency; CC threshold α.

Output: Cluster indexes of all CIR sequences, ***Labels***.

```
Labels ← 0; ClusterID ← 1;
find the maximum of R, LargestCC and its coordinate (i, j);
while LargestCC > α do
    if Labels(i) and Labels(j) are both 0
        Assigning ClusterID to Labels(i) and Labels(j);
        ClusterID ← ClusterID+1;
    if one of Labels(i) and Labels(j) is not 0
        Assigning the the value of the nonzero one to the other one;
    R(i, j)←0;
    find the maximum of R, LargestCC and its coordinate (i, j);
end
```

It always finds a pair of CIR sequences with the highest similarity by searching the maximum of CC matrix. If both two CIR sequences have not been grouped into clusters, they are labeled with the same new cluster index. If one of the two CIR sequences has been grouped into a cluster, the other one is grouped into the same cluster. If both two CIR sequences have been grouped into clusters, the algorithm does nothing. Then, the CC matrix is updated by setting current maximum to 0. The above process is repeat until the maximum of CC matrix is not large enough.

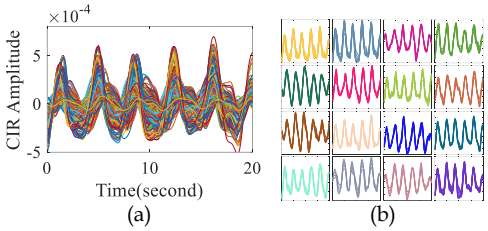

Fig. 10. Compact CIR sequence clusters

Fig. 10(a) shows all the periodical CIR sequences of three subjects who breathe with the same frequency about 17 bpm but different phases (phase interval is about π / 3). Fig. 10(b) shows part of CIR sequence clusters obtained from Algorithm 1. We observe that within each cluster, CIR sequences are very similar. The algorithm can find all the compact CIR sequences clusters and the outlier CIR sequences will be removed automatically. Generally, the parameter α should be set within 0.94~0.98 to ensure that the CIR sequences in the same cluster corresponding to the same part of a subject's chest.

6.2.2 Second-stage Clustering

To reduce computation burden, we firstly compress each CIR cluster as its mean vector. The idea of the second-stage clustering algorithm is inspired by the fact that the mean vectors belonging to different subjects have obviously different phases, thus they hardly occur simultaneously in the neighborhood of one mean vector. The second-stage clustering algorithm operates on CC matrix of mean vectors to find non-overlapping neighbourhoods of mean vector. Algorithm 2 shows the detailed process.

Algorithm 2: *Second stage clustering algorithm*

Input: CC matrix $\boldsymbol{R}$ of the mean vectors of CIR sequence clusters obtained in first stage clustering; CC threshold α.

Output: Cluster indexes of all mean vectors, ***Labels***.

```
Nums ← count the elements > α in each row of R;
sort rows of R based on Nums in descending order;
Labels ← 0; ClusterID ← 1; tempSet is initialized to empty;
for i from 1 to M do //M is the size of R which is a square matrix.
    Indices ← get column indices of elements > α in the ith row of R;
    if the intersection of Indices and tempSet is empty
        Labels(Indices) ← ClusterID; ClusterID ← ClusterID+1;
        add Indices into tempSet;
    end
end
```

Firstly, the CC matrix (each row or column corresponds to a mean vector) is reorganized by rows in descending order of the sizes of the neighbourhoods of all mean vectors. CC matrix reorganization facilitates prioritizing the discovery of large mean vector clusters, which is helpful to

improve clustering accuracy in the next step [62]. Finally, the neighborhood of the mean vector is found sequentially by row. If the current neighbourhood is not overlapped with the reserved neighbourhoods, it will be also reserved and the mean vectors in the current neighborhood are labeled as a new cluster.

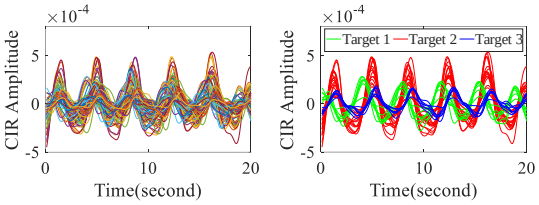

Fig. 11. Clusters of the mean vectors of the CIR clusters

Fig. 11(a) shows all mean vectors of the CIR sequence clusters generated in the first stage. Fig. 11(b) shows the mean vector clusters obtained from Algorithm 2. We observe that Algorithm 2 successfully separates the mean vectors belonging to three subjects. Generally, the parameter CCThrd should be set to a range between 0.9 to 0.94 to ensure that the CIR sequence mean vectors corresponding to different parts of the same chest will be merged while preventing the mean vectors for different subjects being merged.

6.3 Breath Wave Recovering and Subject Counting

With the method presented in Section 5, CIR sequences can be grouped by frequency. Then, by applying two-stage CIR sequences clustering algorithm on each group, we can get mean vector clusters corresponding to each subject. The breath wave of each subject can be recovered as the mean vector of each cluster. Besides, the number of subjects can be estimated as the total number of CIR groups.

7 Evaluation

In this section, we conduct comprehensive experiments to evaluate *MultiResp*. We compare *MultiResp* with the baseline in both single- and multi-user scenarios. We then evaluate *MultiResp* in a range of challenging scenarios: 1) subjects breathe with the same rate and similar rates, 2) subjects face away from the transceiver and are blocked by furniture or other targets, and 3) the number of subjects change dynamically. Additionally, we test the effective sensing distance and impact of apnea, ambient noise, body movement and different clothes. We also extend our experiments to animals. Finally, we discuss the limitations of the system. We have made a demo video which contains the video clips of all the experiments. It is available at https://tinyurl.com/2p9c93v3 and https://youtu.be/naB3rFrNSfE.

7.1 Experimental Settings

7.1.1 Prototype Implementation and Parameter Settings

We implement a prototype system on an ultrasonic transceiver and a laptop computer (Thinkpad T450 with Intel Core i5-5200 CPU, 8G RAM). The hardware setting is shown in Fig. 12. The transceiver consists of a USB sound card embedded with two broadband omnidirectional microphones and four speakers spaced $\pi/2$ apart. The software system is implemented in MATLAB to run the respiration monitoring algorithm, and control speakers and microphones through the sound card. Transmitted signal has the following parameter settings: $f_c = 26KHz, B = 2KHz, T = 0.04s, T' = 0.1s$ (the duration of *MultiResp* executing for one time is equal to T'). The sampling rate of transceiver $f_s = 96$KHz. The power and sensitivity of the speaker are 50 watt and 94dB, respectively. The beamwidth of the speaker $f_c = 26KHz$ is $\pm 14°$. The sensitivity, signal-to-noise ratio and the total harmonic distortion of the mic are -26 dBFs, 64.3 dB and 0.2%, respectively.

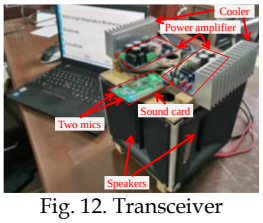

Fig. 12. Transceiver

7.1.2 Baseline and Ground Truth

We compare *MultiResp* with RespTracker [56], which is the state-of-the-art acoustic multi-user respiration monitoring approach. For a fair comparison, the baseline is implemented using the same devices and the same parameter settings as specified in [56].

Each subject is asked to wear a commercial motion sensor WitMotion WT901WIFI on the abdomen, which integrates a 3-axis acceleration sensor, a gyroscope, a 3-axis angle sensor, and a magnetometer. It accurately captures chest movement during breathing for the ground truth in each experiment. In addition, all the experiments are recorded by a camera (Mi 360° Home Security Camera 2K Pro).

7.2 Performance

7.2.1 Comparison with The Baseline

7.2.1.1 Single-user scenario

We recruit 3 participants to evaluate the performance of *MultiResp* in single-user scenario. In each setup, a subject is randomly located in a room (5.2m x 3m x 3.5m). Fig. 13(a) shows the room layout and the location and orientation of three subjects. Each experiment runs for 10 minutes, we record the breath rates estimated by *MultiResp* and the baseline system, respectively.

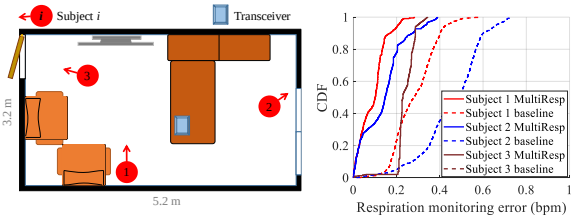

Fig. 13. Settings and results of single user scenario.

Fig. 13(b) shows the cumulative distribution function

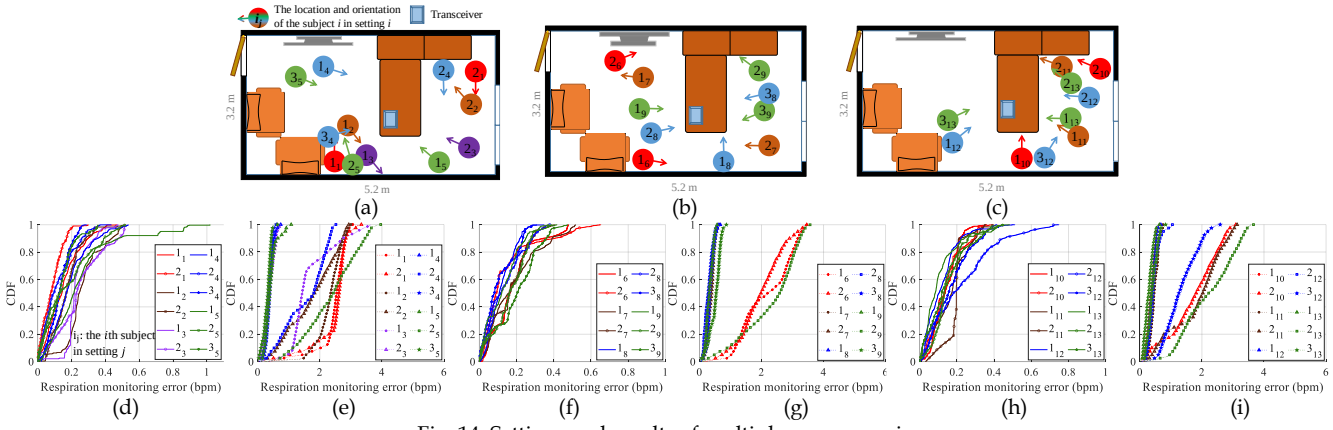

Fig. 14. Settings and results of multiple user scenarios.

(CDF) of respiration monitoring error of both *MultiResp* and the baseline. We observe that the maximum respiration error of *MultiResp* is smaller than 0.4 bpm for all subjects. The baseline works well for subjects 1 and 2 and fails for subject 3 who faces away from the transceiver.

7.2.1.2 Multiple users breathing with different breath rates

To test the performance when multiple subjects breathe with different rates, we conduct 3 groups of experiments where the breath rate differences are set as 1 bpm, 2 bpm, and larger than 2 bpm, respectively. Each group contains at least 4 different experimental settings. In each setting, subjects breathe with different breath rates as shown in Table 1. $(x, y)_i$ denotes that there are two subjects in setting i and they breathe with rate x bpm and y bpm, respectively. $(x, y, z)_i$ denotes that there are three subjects in setting i and they breathe with rate x bpm, y bpm and z bpm, respectively. Fig. 14(a)-(c) show the room layout, subject location and orientation in each group, respectively. Because the baseline has to know number of subjects in advance, in each setting, we manually feed this value into the baseline.

TABLE 1 TARGETS BREATH RATE IN THREE GROUP

ΔBr (bpm)	Br of 2 targets (bpm)	Br of 3 targets (bpm)
1	$(13, 14)_1$, $(17, 18)_2$, $(19, 20)_3$	$(13, 14, 15)_4$, $(17, 18, 19)_5$
2	$(12, 14)_6$, $(15, 17)_7$	$(13, 15, 17)_8$, $(16, 18, 20)_9$
>2	$(14, 17)_{10}$, $(15, 19)_{11}$	$(12, 15, 19)_{12}$, $(13, 17, 20)_{13}$

Br = breath rate;

Fig. 14(d), (f) and (h) show the CDF of respiration monitoring error of *MultiResp* of three groups (i_j denotes the i-th subject in setting j.). Fig. 14(e), (g) and (i) show the CDF of respiration monitoring error of baseline of three groups. We observe that the maximum errors and median errors of *MultiResp* in all three group are smaller than 1 bpm and 0.3 bpm, respectively. The baseline works well partially, and its maximum error is larger than 2.5 for subjects 1_1, 1_2, 2_1, 2_2, 1_3, 2_4, 2_5, 1_6, 2_6, 1_7, 2_9, 2_{10}, 2_{11}, 3_{12}, 2_{13}. Especially for subject 1_7 who faces away from the transceiver, the baseline completely fails. This is because the baseline relies on the distance from subjects' chest to the transceiver. However, when subjects are not facing towards to the transceiver, the multipath signals reflected from the same subject chest propagate along different paths, and the time delays of these signals are not able to form clear and stable distance information. Differently, *MultiResp* selects reflected signals by a globle search method based on CIR sequence periodicity, then groups these multipath signals by frequency and phase, finally forms breath waves by merging the variation of multipath signals in each group.

7.2.2 Experiments in Various Challenging Scenarios

7.2.2.1 Subjects breathing with very similar rates

MultiResp is able to distinguish very similar breath rates using the high-resolution CIR frequency measuring algorithm. We conduct an experiment to test the smallest breath rate difference that *MultiResp* can distinguish. In each experiment, two subjects are required to keep a specific breath rate difference. We repeat the experiment for 7 times and the breath rate difference is set in a descending order from 0.8 bpm to 0.2 bpm. To facilitate, two subjects follow a smartphone application metronome which gives an instruction for breathing. Experimental results show that *MultiResp* is able to distinguish breath rate difference larger than 0.4 bpm.

Fig. 15(a) shows the result when two subjects breathe with 18.4 bpm and 19 bpm. Fig. 15(b) shows the result when two subjects breathe with 12 bpm and 12.4 bpm. We observe that *MultiResp* robustly distinguishes these similar breath rates.

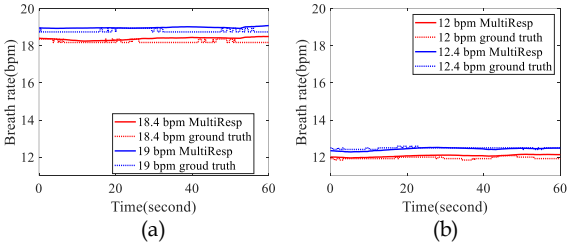

Fig. 15. Recorded breath rates of two subjects breathing with similar rates

7.2.2.2 Subjects breathing with the same rate

To test the performance when multiple subjects breathe with same rate, we conduct experiments in three settings. Table 2 shows breath rate, number of subjects, and breath phase difference between subjects in each setting. To facilitate, subjects follow a smartphone metronome App which gives an instruction to breathe in the same rate. Fig. 16(a) shows the room layout, subject location and orientation in

each setting. Fig. 16 (b) show the scenario of setting 2. From Fig. 16(b), we observe that the user interface of *MultiResp* shows both the detected respiration rates and the number of subjects breathing with each rate.

TABLE 2 BREATH RATE OF DIFFERENCE

Setting num.	*Br* (bpm)	Targets amount	Breath phase difference
1	15	2	$\pi/3$
2	13	3	$\pi/4$
3	16	3	$\pi/4$

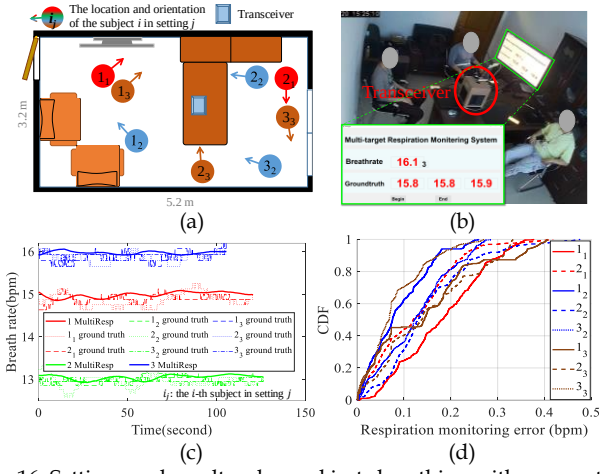

Fig. 16. Settings and results when subjects breathing with same rate.

Fig. 16(c) shows the tracked breath rates over time and the ground truth in three settings. Fig. 16(d) shows the CDF of respiration monitoring error derived from Fig. 16(c). We observe that maximum errors and median errors of *MultiResp* in all three settings are smaller than 0.5 bpm and 0.2 bpm, respectively.

7.2.2.3 Subjects facing away from transceiver

In this experiment, we evaluate the performance of *MultiResp* when subjects face away from the transceiver with 3 different settings: 1) two subjects face away from the transceiver and breathe naturally, 2) three subjects face away from transceiver and breathe naturally, 3) two subjects face away from transceiver and breathe with the same rate.

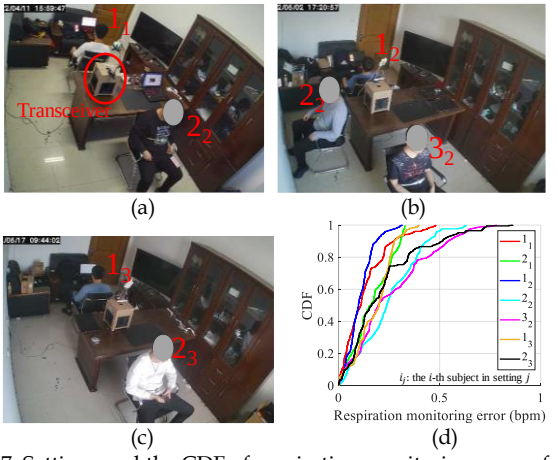

Fig. 17. Settings and the CDF of respiration monitoring error of *MultiResp* when subjects face away from transceiver.

Fig. 17(a)~(c) show the scenarios of three settings respectively. Fig. 17(d) shows the CDF of respiration monitoring error of all subjects in three settings. We observe that the maximum errors and median errors of *MultiResp* in all settings are all smaller than 0.9 bpm and 0.3 bpm, respectively.

7.2.2.4 Subjects blocked by furniture or other subjects

In this experiment, we evaluate *MultiResp* when subjects are blocked by furniture or other subjects. Specifically, we test *MultiResp* with 9 different settings. Fig. 18(a)~(d) show the scenarios that single subject is blocked by furniture. Fig. 18(e) and 18(g) show the scenarios that multiple subjects are blocked by furniture. Fig. 16(h) and 18(i) show the scenarios that subjects are blocked by other targets. Fig. 18(f) shows a scenario that the subjects are not only blocked by furniture but also blocked by other subjects. Additionally, the two subjects in setting 7 (i.e., Fig. 18(g)) breathe with the same rate.

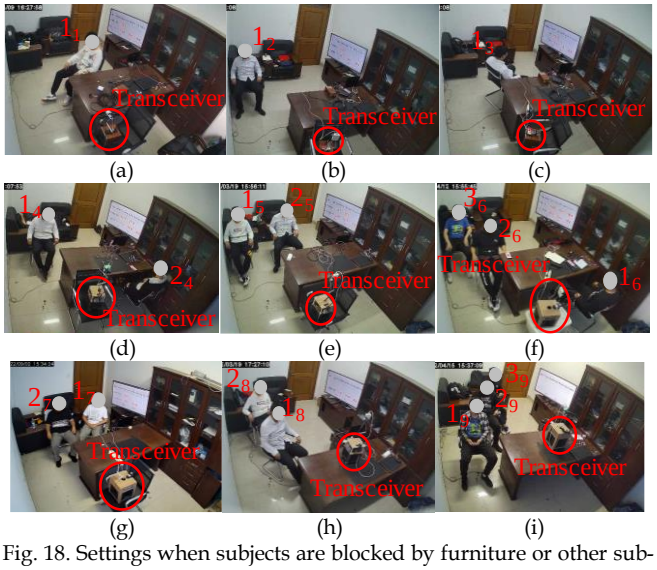

Fig. 18. Settings when subjects are blocked by furniture or other subjects.

Fig. 19 shows the CDF of respiration monitoring error of *MultiResp* in all settings. We observe that except for the second subject in setting 9 (i.e., the subject labeled with 2_9 shown in Fig. 18(i)), the maximum error and median error of *MultiResp* in all other settings are smaller than 0.85 bpm and 0.3 bpm, respectively.

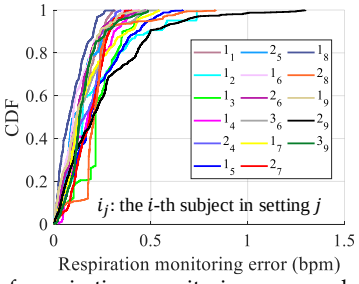

Fig. 19. CDF of respiration monitoring error when subjects are blocked by furniture or other subjects

7.2.2.5 Number of subjects changes dynamically

In this experiment, we evaluate *MultiResp* when the number of subjects changes dynamically with two settings: 1) one subject breathes naturally in the room, then other two subjects enter the room and breathe naturally, finally one of them leaves the room. 2) Three subjects breathe with the same rate, then two of subjects leave the room.

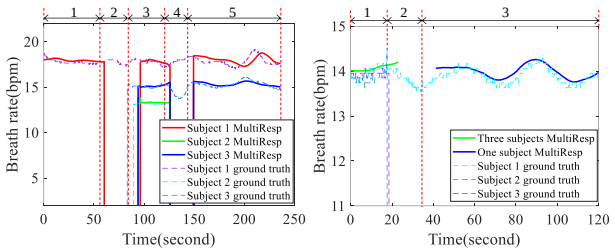

(a) (b)

Fig. 20. The recorded breath rate when subjects number changes dynamically.

Fig. 20 (a) shows the tracked respiration rate over time in setting 1. In time period 1, subject 1 breathes naturally in the test room. *MultiResp* accurately tracks the respiration of subject 1. Then, subjects 2 and 3 enter the room in time period 2. Because of the movement interference, *MultiResp* fails to monitor subjects' respiration. All three subjects breathe naturally in time period 3. *MultiResp* accurately tracks the respiration of both three subjects, however, there is a time delay. It is due to the fact that *MultiResp* needs a time window to estimate the breathing rate. In time period 4 subject 2 leaves the room, while subjects 1 and 3 still breathe naturally. After subject 2 leaves the room, *MultiResp* successfully tracks the breath rates of subject 1 and 3 again.

Fig. 20 (b) shows the tracked respiration rate over time in setting 2 (note that in Fig. 20 (b), the solid lines of different colors represent different number of the subjects). In time period 1, three subjects breathe with the same rate. *MultiResp* accurately counts the number of the subjects and tracks their respiration. In time period 2, subjects 1 and 3 leave the room. Then, *MultiResp* accurately tracks the respiration of subject 2.

From the above results, we can see that *MultiResp* can adapt to dynamical change of target number.

7.2.2.6 Subjects' breathing rate changing dynamically

We conduct experiments with two different settings to evaluate *MultiResp* when subjects breathing rate changes dynamically. 1) Firstly, three subjects breathe with the same rate, one of the subjects then changes his breath rate suddenly. 2) one subject breathes naturally, and another subject increases his breath rate gradually.

Fig. 21(a) shows the breath rate recorded by *MultiResp* in setting 1 (note that in Fig. 21(a), the solid lines of different colors denote different number of the subjects). We can see that during time period 1, *MultiResp* not only correctly counts the number of subjects but also accurately tracks their respiration rates. At the end of time period 1, the breath rate of subject 3 changes suddenly. The sudden change leads to both the ground truth and *MultiResp* fail to track the breath rate of subject 3 for about 20 seconds. After that, *MultiResp* successfully tracks the breath rate. Then, three subjects again. Fig. 21(b) shows the breath rate recorded in setting 2. We see that *MultiResp* is able to accurately track the respiration when subject's breath rate changes gradually.

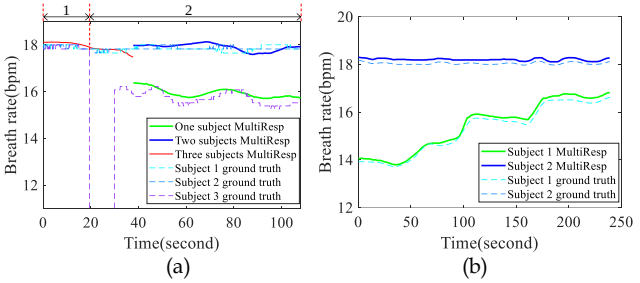

(a) (b)

Fig. 21. The recorded breath rate when subjects' breath rate changes dynamically.

7.2.3 Long Term Evaluation

To test the stability of *MultiResp*, we conduct an experiment for about 2 hours in a room (8.4 m×5.8 m×3.4m). Fig. 22 (a) shows the real scenario. Two participants sleep in the room. Fig. 22(b) shows the CDF of respiration monitoring error. We can see that the median and maximum error are smaller than 0.2 bpm and 0.5 bpm, respectively.

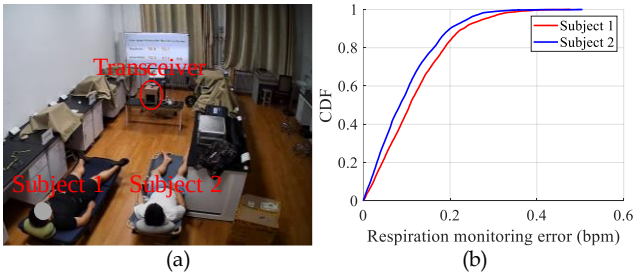

(a) (b)

Fig. 22. The recorded breath rate when subjects' breath rate changes dynamically.

7.3 Robustness testing

7.3.1 Impact of Apnea

Detecting Apnea is an important objective of monitoring respiration during sleep. We conduct experiments with two different settings to evaluate whether *MultiResp* can detect Apnea. 1) Three subjects breathe naturally, then one of them holds breath for a while to simulate Apnea, and finally, resumes to breathe naturally. 2) There are totally three subjects. Subjects 1 and 2 breathe with the same rate and subject 3 breathe with a different rate. Then, subject 2 holds breath for a while to simulate Apnea and resumes to breathe.

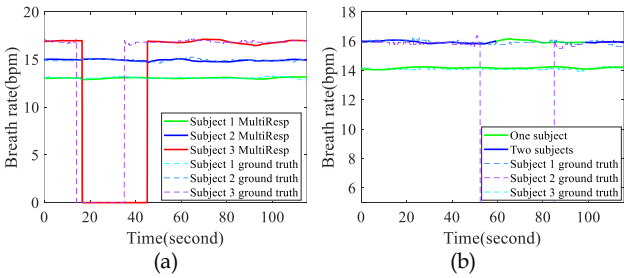

(a) (b)

Fig. 23. The recorded breath rate when Apnea happens.

Fig. 23(a) shows the breath rate in setting 1. We can see that *MultiResp* detects the Apnea of subject 3 and accurately tracks the respiration of other two subjects. However, time delay occurs at both the start and end of Apnea. Fig. 23(b) shows the respiration rate in setting 2 (the solid lines of different colors denote different number of the subjects). We can see that *MultiResp* detects the Apnea of subject 2 even subjects 1 and 2 breathe with the same rate, and accurately tracks the respiration of other two subjects. However, time delay still occurs.

When subject number changes, i.e., subjects enter or leave the room during respiration monitoring, *MultiResp* fails for all subjects due to body movement (refer to Sec. 7.2.2.5). This is because body movement heavily changes the multipath signals and finally results in CIR irregular fluctuation. Differently, when Apnea happens, *MultiResp* can still accurately tracks the respiration of the subjects without Apnea.

7.3.2 Impact of Noise and Body Movement

Ambient noise and body movement are two main interference sources. In this experiment, we evaluate their impact in two settings: 1) two subjects breathe naturally and the loudspeaker on the laptop plays music with different decibels. 2) Three subjects breathe naturally. Then, one of the subjects shakes his hands for a while.

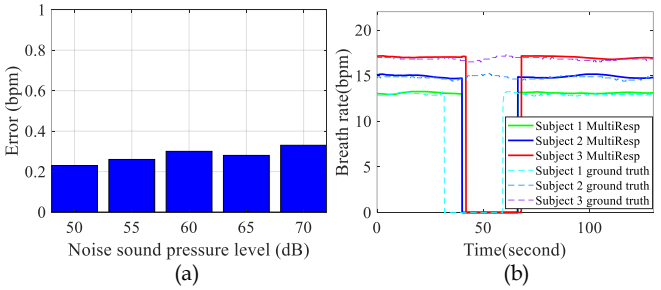

Fig. 24. The recorded breath rate when this is movement or noise interference.

Fig. 24(a) shows the median value of respiration monitoring error under different noise levels. We can see that even when the noise level reaches 70 dB, the median error is lower than 0.4 bpm. Fig. 24(b) shows the breath rate of three subjects in setting 2. We can see that when subject 1 shakes his hand, *MultiResp* fails for all subjects. However, after hands shaking, *MultiResp* is able to recover respiration monitoring after a while.

7.3.3 Imapat of Different Clothes

We conduct experiments with two different settings to evaluate the impact of different clothes including down coat, knitwear, shirt and t-shirt. In each setting, two subjects are recruited to wear different clothes. In setting 1, two subjects wear down coat and shirt, respectively. In setting 2 two subjects wear knitwear and t-shirt, respectively.

Fig. 25(a) and Fig. 25(b) show the scenarios of two settings. Fig. 25(c) shows the CDF of respiration monitoring error when subjects wearing different clothes. We can see that the median and maximum error are smaller than 0.2 bpm and 0.7 bpm, respectively.

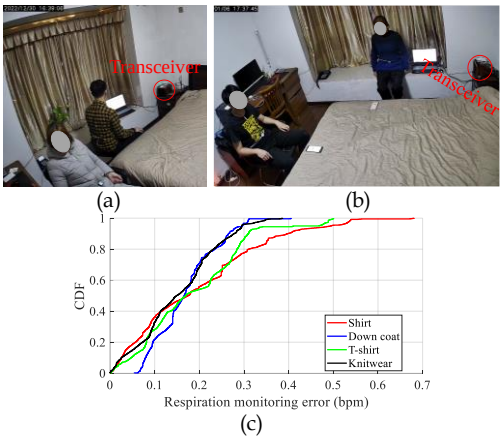

Fig. 25. Settings and the CDF of respiration monitoring error when subjects wear different clothes.

7.3.4 Imapat of Transmitting Power

We also conduct experiments to evaluate the impact of transmitting power. Two subjects are recuited to evaluate the performance under different transmitting power. To ensure the sound pressure is the same for two subjects, the distances from two subjects to the transceiver remains the same. We adjust the transmitted power to make sound pressure measured at the location of subjects are 45 dB, 50 dB, 55 dB, 60 dB, 65 dB, 70 dB and 75 dB in each setting, respectively. *MultiResp* fails when the sound pressure is 45 dB and 50 dB. Fig. 26 shows the CDF of respiration monitoring error under other sound pressures. We can see that the median error is lower than 0.3 bmp. So it is suggested to keep the sound pressure lager than 50 dB.

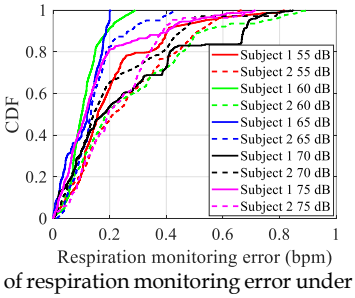

Fig. 26. The CDF of respiration monitoring error under different transmitting power.

7.4 Evaluation with animals

In this experiment, we evaluate *MultiResp* on animals (i.e., goat). Compared to human skin, goat wool absorbs most of the acoustic signal, resulting in very weak reflections.

Fig. 27. Two real scenarios to evaluate *MultiResp* with goats.

Fig. 27(a) and 27(b) show two examples of real scenarios. To prevent the devices from being damaged by goats, we

separate the devices and goats using a table. Fig. 27(a) shows that the two goats are located closely and are blocked by the table. Additionally, it is difficult to place the belt on goats for capturing the ground truth because the goats always bite it off. Instead, we obtain the ground truth by replaying video. To facilitate breath counting, we mark the goats with black tape on their abdomen. Thus, when goats breathe, we can easily count the breath by observing the shape change of black tape.

Table 3 shows the results. The time that goat completely falls asleep is very short. Even its eyes are closed, its ears and tail wag now and then. So, it is difficult to find a long time that all the goats completely fall asleep. We totally capture four time slices that all goats completely fall asleep. During these four time slices, the maximum error of respiration monitoring is one breath.

TABLE 3 EVALUATION RESULT WITH GOATS

Goat ID	Monitoring time (mm:ss)	Ground truth (Breaths)	*MultiResp* (Breaths)	Error (Breaths)
845	01:29	23	24	1
100		27	27	0
44	01:34	25	25	0
144		30	31	1
849	01:09	17	16	-1
23		21	21	0
32		23	23	0
963	00:56	19	20	1
871		15	15	0
943		17	18	1

7.5 Effective sensing distance estimation

In this experiment, we evaluate *MultiResp* with respect to sensing distance varies from 3 to 10m. We have two settings: subject faces the transceiver, and subject faces away from the transceiver. The detailed parameters of the transceiver are presented in Sec. 7.1.1. Fig. 28(a) shows the real scenarios. Fig. 28(b) shows median value of respiration monitoring error at different distances. We can see that when subject faces to the transceiver, the median error is smaller than 1 bpm within 8 meters. When subject faces away from the transceiver, the median error is smaller than 1 bpm within 6 meters.

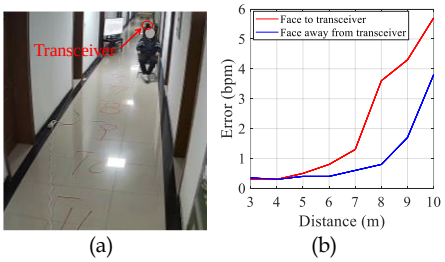

(a) (b)

Fig. 28. Effective sensing distance estimation.

7.6 Limitations

1) Not suitable for too large rooms. *MultiResp* may fail to monitor respiration if the room is too large. We know that too large room might result in weaker multipath reflection, which leads to low SNR and finally cause respiration monitoring failing.

2) Time delay. Even though *MultiResp* can 1) adapt to dynamical subject number change, 2) detect Apnea, 3) automatically recover to monitor respiration after body movement, it introduces a time delay about 10 seconds because *MultiResp* requires a time window to estimate the breath rate.

8 CONCLUSION

This paper presents *MultiResp*, an acoustic based multi-user respiration monitoring system. By leveraging abundant multipath signals reflected indirectly from subjects' chests, *MultiResp* is able to accurately monitor the respiration of subjects even they face away from the transceiver or are blocked. By extracting the fine-grained breathing rates and phase difference between subjects, *MultiResp* can separate the breath waves with the same or similar rates and adapt to dynamical change of subject number during monitoring. Extensive experiments show that *MultiResp* is highly accurate with a median error of 0.3 bpm in various scenarios.

ACKNOWLEDGMENT

The authors would like to express their special appreciation to the volunteers for participating in our experiments. The ethics approval has been obtained in prior to all the experiments. This work was supported in part by the Key Research and Development Project in Shaanxi Province of China (2023-YBGY-257), the Shaanxi Key Industry Innovation Chain Project (2023-ZDLNY-69) and the Yangling Livestock Industry Innovation Center Double-chain Fusion Project (2022GD-TSLD-46).

REFERENCES

[1] R. Paradiso,"Wearable health care system for vital signs monitoring," 4th International IEEE EMBS Special Topic Conference on Information Technology Applications in Biomedicine, pp. 283-286, Apr. 2003, doi:10.1109/ITAB.2003.1222533.

[2] S. Javaheri, T. J. Parker, J. D. Liming, W. S. Corbett, H. Nishiyama, L. Wexler, andG. A. Roselle, "Sleep apnea in 81 ambulatory male patients with stable heart failure: types and their prevalences, consequences, and presentations," Circulation, vol. 97, no. 21, pp. 2154-2159, Jun. 1998, doi:10.1161/01.CIR.97.21.2154.

[3] D. Norman and J S. Loredo. "Obstructive sleep apnea in older adults," Clinics in geriatric medicine, vol. 24, no. 1, pp. 151-165, Feb. 2008, doi: 10.1016/j.cger.2007.08.006.

[4] J. N. Wilkinson and V. U. Thanawala, "Thoracic impedance monitoring of respiratory rate during sedation–is it safe?" Anaesthesia, vol. 64, no. 4, pp. 455-456, Mar. 2009, doi:10.1111/j.1365-2044.2009.05908.x.

[5] M. B. Jaffe. "Infrared measurement of carbon dioxide in the human breath: "breathe-through" devices from Tyndall to the present day," Anesthesia & Analgesia 107.3 (2008), vol. 107, No. 3, pp. 890-904, Sep. 2008, doi:10.1213/ane.0b013e31817ee3b3.

[6] N. H.Shariati and E. Zahedi, "Comparison of selected parametric models for analysis of the photoplethysmographic signal," 1st International Conference on Computers, Communications, & Signal Processing with Special Track on Biomedical Engineering, pp. 169-172, Nov. 2005, doi: 10.1109/CCSP.2005.4977182.

[7] S. Wiesner and Z. Yaniv, "Monitoring patient respiration using a single

optical camera," 29th Annual International Conference of the IEEE Engineering in Medicine and Biology Society, pp.2740-2743, Oct. 2007, doi: 10.1109/IEMBS.2007.4352895.

[8] S. Nukaya, T. Shino, Y. Kurihara, K. Watanabe, and H. Tanaka. "Noninvasive bed sensing of human biosignals via piezoceramic devices sandwiched between the floor and bed," IEEE Sensors journal, vol. 12, No. 3, pp.431-438, Nov. 2010, doi: 10.1109/JSEN.2010.2091681.

[9] K.Watanabe, T. Watanabe, H. Watanabe, H. Ando,T. Ishikawa, and K. Kobayashi. "Noninvasive measurement of heartbeat, respiration, snoring and body movements of a subject in bed via a pneumatic method," IEEE transactions on biomedical engineering, vol. 52, No. 12, pp. 2100-2107, Nov. 2005, doi:10.1109/TBME.2005.857637.

[10] M. B. Norman, S. Middleton, O. Erskine, P. G. Middleton, J. R. Wheatley, and C. E. Sullivan. "Validation of the Sonomat: a contactless monitoring system used for the diagnosis of sleep disordered breathing," Sleep, vol. 37, No. 9, pp. 1477-1487, Sep. 2014, doi:10.5665/sleep.3996.

[11] Z. Chen, Ju Teng Teo, Soon Huat Ng, and H. Yim, "Smart pillow for heart-rate monitoring using a fiber optic sensor.," Optical Fibers, Sensors, and Devices for Biomedical Diagnostics and Treatment XI, pp. 9-15, Feb. 2011, doi:10.1117/12.871208.

[12] S. Šprager and Z.Damjan, "Heartbeat and respiration detection from optical interferometric signals by using a multimethod approach," IEEE transactions on biomedical engineering, vol. 59, No. 10, pp. 2922-2929, Oct. 2012, doi:10.1109/TBME.2012.2213302.

[13] J.Penne, C. Schaller, J. Hornegger, and T. Kuwert, "Robust real-time 3D respiratory motion detection using time-of-flight cameras," International Journal of Computer Assisted Radiology and Surgery, vol. 3, No. 5, pp. 427-431, Jul. 2008, doi:10.1007/s11548-008-0245-2.

[14] D. Obeid, G. Zaharia, S. Sadek, and Ghaïs El Zein, "Cardiopulmonary activity monitoring with contactless microwave sensor," Mediterranean Microwave Symposium 2012, pp. 1-4, Sept. 2012, doi: hal-00734895.

[15] Y. Hou, Y. Wang, and Y. Zheng, "TagBreathe: Monitor breathing with commodity RFID systems," 2017 IEEE 37th International Conference on Distributed Computing Systems (ICDCS), pp. 404-413, Jul. 2017, doi:10.1109/ICDCS.2017.76.

[16] L. Chen, J. Xiong, X. Chen, Sunghoon Ivan Lee, D. Zhang, T. Yan, and D. Fang, "LungTrack: Towards contactless and zero dead-zone respiration monitoring with commodity RFIDs," Proceedings of the ACM on Interactive, Mobile, Wearable and Ubiquitous Technologies, vol. 3, No. 3, pp. 1-22, Sept. 2019, doi:10.1145/3351237.

[17] Z. Hussain, S. Sagar, W. Zhang, and Q. Sheng, "A cost-effective and non-invasive system for sleep and vital signs monitoring using passive RFID tags," Proceedings of the 16th EAI International Conference on Mobile and Ubiquitous Systems: Computing, Networking and Services, pp. 153-161, Nov. 2019, doi:10.1145/3360774.3360797.

[18] A.D. Droitcour, O. Boric-Lubecke, and G. T. A. Kovacs, "Signal-to-noise ratio in Doppler radar system for heart and respiratory rate measurements," IEEE transactions on microwave theory and techniques, vol. 57, No. 10, pp. 2498-2507, Oct. 2009, doi:10.1109/TMTT.2009.2029668.

[19] A.D. Droitcour, O. Boric-Lubecke, V.M. Lubecke, J. Lin, and G. T. A. Kovacs, "Range correlation and I/Q performance benefits in single-chip silicon Doppler radars for noncontact cardiopulmonary monitoring," IEEE Transactions on Microwave Theory and Techniques, vol. 52, No. 3, pp. 838-848, Mar. 2004, doi:10.1109/TMTT.2004.823552.

[20] R. Fletcher and J. Han, "Low-cost differential front-end for Doppler radar vital sign monitoring," IEEE MTT-S International Microwave Symposium Digest, pp. 1325-1328, Jul. 2009, doi:10.1109/MWSYM.2009.5165949.

[21] Z. Yang, M. Bocca, V. Jain, and P. Mohapatra, "Contactless breathing rate monitoring in vehicle using UWB radar," Proceedings of the 7th international workshop on real-world embedded wireless systems and networks, pp. 13-18, Nov. 2018. , doi:10.1145/3277883.3277884.

[22] S. Venkatesh, C.R. Anderson, N.V. Rivera, and R.M. Buehrer, "Implementation and analysis of respiration-rate estimation using impulse-based UWB," IEEE Military Communications Conference, pp. 3314-3320, Oct. 2005. , doi:10.1109/MILCOM.2005.1606167.

[23] M. Baboli, O. Boric-Lubecke, and V. Lubecke, "A new algorithm for detection of heart and respiration rate with UWB signals," Annual International Conference of the IEEE Engineering in Medicine and Biology Society, pp. 3947-3950, Aug. 2012, doi:10.1109/EMBC.2012.6346830.

[24] M. Baldi, F. Appignani, B. Zanaj, and F. Chiaraluce, "Body movement compensation in UWB radars for respiration monitoring," IEEE First AESS European Conference on Satellite Telecommunications, pp. 1-6, Oct. 2012, doi:10.1109/ESTEL.2012.6400084.

[25] M. Mercuri, G. Sacco, R. Hornung, P. Zhang, H. J. Visser, M. Hijdra, and Yao-Hong L, "2-D localization, angular separation and vital signs monitoring using a SISO FMCW radar for smart long-term health monitoring environments," IEEE Internet of Things Journal, pp. 11065-11077, vol. 8, no. 14, Jan. 2021. , doi:10.1109/JIOT.2021.3051580.

[26] H. Abdelnasser, K.A. Harras and M. Youssef, "UbiBreathe: A ubiquitous non-invasive WiFi-based breathing estimator," Proceedings of the 16th ACM International Symposium on Mobile Ad Hoc Networking and Computing, pp. 277-286, Jun. 2015, doi:10.1145/2746285.2755969.

[27] R. Ravichandran, E. Saba, K.Y. Chen, R. Ravichandran, E. Saba, and K.Y. Chen, "WiBreathe: Estimating respiration rate using wireless signals in natural settings in the home," IEEE International Conference on Pervasive Computing and Communications, pp. 131-139, Jul. 2015, doi:10.1109/PERCOM.2015.7146519.

[28] N. Patwari, L. Brewer, Q. Tate, O. Kaltiokallio, and M. Bocca, "Breathfinding: A wireless network that monitors and locates breathing in a home," IEEE Journal of Selected Topics in Signal Processing, vol. 8, no. 1, pp. 30-42, Nov. 2013, doi:10.1109/JSTSP.2013.2287473.

[29] Xuefeng L, Jiannong C, Shaojie T, and Jiaqi W, "Wi-sleep: Contactless sleep monitoring via WiFi signals," IEEE Real-Time Systems Symposium, pp. 346-355, Jan. 2014, doi:10.1109/RTSS.2014.30.

[30] Y. Hao, J. Li, W. Wang and Q. Lin, "An Animal Respiration Monitoring System Based on Channel State Information of Wi-Fi Network," Proceedings of the 2019 7th International Conference on Information Technology: IoT and Smart City, pp. 283-289, Dec 2019, doi:10.1145/3377170.3377196.

[31] X. Wang, Y. Chao, and S. Mao, "On CSI-based vital sign monitoring using commodity WiFi," ACM Transactions on Computing for Healthcare 1.3, vol. 1, no. 3, pp. 1-27, May. 2020, doi:10.1145/3377165.

[32] X. Liu, J. Cao, S. Tang, J. Wen, and P. Guo, "Contactless respiration monitoring via off-the-shelf WiFi devices," IEEE Transactions on Mobile Computing, vol. 15, no. 10, pp. 2466-2479, Dec. 2015, doi:10.1109/TMC.2015.2504935.

[33] C. Wu, Z. Yang, Z. Zhou, X. Liu, Y. Liu, and J. Cao, "Non-invasive detection of moving and stationary human with WiFi," IEEE Journal on Selected Areas in Communications, vol. 33, no. 11, pp. 2329-2342, May. 2015, doi:10.1109/JSAC.2015.2430294.

[34] J. Liu, Y. Wang, Y. Chen, J. Yang, X. Chen, and J. Chen, "Tracking vital signs during sleep leveraging off-the-shelf WiFi," Proceedings of the 16th ACM international symposium on mobile ad hoc networking and computing, pp. 267-276, Jun 2015, doi:10.1145/2746285.2746303.

[35] D. Zhang, H. Wang, and D. Wu, "Toward centimeter-scale human activity sensing with Wi-Fi signals," Computer, vol. 50, no. 1, pp. 48-57, Jan. 2017, doi:10.1109/MC.2017.7.

[36] K. Niu, F. Zhang, Z. Chang, and D. Zhang, "A fresnel diffraction model

based human respiration detection system using COTS Wi-Fi devices," Proceedings of the 2018 ACM International Joint Conference and 2018 International Symposium on Pervasive and Ubiquitous Computing and Wearable Computers, pp. 416-419, Oct. 2018, doi:10.1145/3267305.3267561.

[37] Y. Zeng, E. Yi, D. Wu, R. Gao, and D. Zhang, "A full human respiration detection system using commodity Wi-Fi devices," Proceedings of the 2018 ACM International Joint Conference and 2018 International Symposium on Pervasive and Ubiquitous Computing and Wearable Computers, pp. 480-483, Oct. 2018, doi:10.1145/3267305.3267560.

[38] Y. Zeng, D. Wu, R. Gao, T. Gu, and D. Zhang, "FullBreathe: Full human respiration detection exploiting complementarity of CSI phase and amplitude of WiFi signals," Proceedings of the ACM on Interactive, Mobile, Wearable and Ubiquitous Technologies, vol. 2, no. 3, pp. 1-19, Sep. 2018, doi:10.1145/3264958.

[39] F. Zhang, D. Zhang, J. Xiong, H. Wang, K. Niu, B. Jin, and Y. Wang, "From Fresnel Diffraction Model to Fine-grained Human Respiration Sensing with Commodity Wi-Fi Devices," Proceedings of the ACM Interactive Mobile Wearable & Ubiquitous Technologies, pp. 1-23, Mar. 2018, doi:10.1145/3191785.

[40] R. Nandakumar, S. Gollakota, and N. Watson, "Contactless sleep apnea detection on smartphones," Proceedings of the 13th annual international conference on mobile systems, applications, and services, pp. 45-57, May. 2015, doi:10.1145/2742647.2742674.

[41] S.D. Min, J.K. Kim, H.S. Shin, Y.H. Yun, C.K. Lee, and M. Lee, "Noncontact respiration rate measurement system using an ultrasonic proximity sensor," IEEE sensors journal, vol. 10, no. 11, pp. 1732 – 1739, Nov. 2010, doi:10.1109/JSEN.2010.2044239.

[42] T. Wang, D. Zhang, Y. Zheng, T. Gu, X. Zhou, and B. Dorizzi, "C-FMCW based contactless respiration detection using acoustic signal," Proceedings of the ACM on Interactive, Mobile, Wearable and Ubiquitous Technologies, vol. 1, no. 4, pp. 1 – 20, Dec. 2018, doi:10.1145/3161188.

[43] P. Arlotto, M. Grimaldi, R. Naeck, and J.M. Ginoux. "An ultrasonic contactless sensor for breathing monitoring," Sensors, vol. 14, no. 8, pp. 15371-15386, Aug. 2014, doi:10.3390/s140815371.

[44] T. Wang, D. Zhang, L. Wang, Y. Zheng, T. Gu, B. Dorizzi, and X. Zhou, "Contactless respiration monitoring using ultrasound signal with off-the-shelf audio devices," IEEE Internet of Things Journal, vol. 6, no. 2, pp. 2959 - 2973, Oct. 2018, doi:10.1109/JIOT.2018.2877607.

[45] A. Wang, J.E. Sunshine, and S. Gollakota, "Contactless infant monitoring using white noise," The 25th Annual International Conference on Mobile Computing and Networking, pp. 1-16, Aug. 2019, doi:10.1145/3300061.3345453.

[46] F. Adib, H. Mao, Z. Kabelac, D. Katabi, and R.C. Miller. "Smart homes that monitor breathing and heart rate," Proceedings of the 33rd annual ACM conference on human factors in computing systems, pp. 837-846, Apr. 2019, doi:10.1145/2702123.2702200.

[47] A. Ahmad, J.C. Roh, D. Wang, and A. Dubey, "Vital signs monitoring of multiple people using a FMCW millimeter-wave sensor," IEEE Radar Conference, pp. 1450-1455, Jun. 2018, doi:10.1109/RADAR.2018.8378778.

[48] S. Yue, H. He, H. Wang, H. Rahul, and D. Katabi, "Extracting multi-person respiration from entangled RF signals," Proceedings of the ACM on Interactive, Mobile, Wearable and Ubiquitous Technologies, pp. 1-2, Jun. 2018, doi:10.1145/3214289.

[49] Y. Yang, J. Cao, X. Liu, and X. Liu, "Multi-breath: Separate respiration monitoring for multiple persons with UWB radar," IEEE 43rd Annual Computer Software and Applications Conference, pp. 840-849, Jul. 2019, doi:10.1109/COMPSAC.2019.00124.

[50] H. Wang, D. Zhang, J. Ma, Y. Wang, Y. Wang, D. Wu, T. Gu, and B. Xie, "Human respiration detection with commodity WiFi devices: do user location and body orientation matter?" ACM International Joint Conference on Pervasive and Ubiquitous Computing, pp. 25-36, Sept. 2016, doi:10.1145/2971648.2971744.

[51] X. Wang, C. Yang, and S. Mao, "PhaseBeat: Exploiting CSI phase data for vital sign monitoring with commodity WiFi devices," IEEE 37th International Conference on Distributed Computing Systems, pp. 1230-1239, Jul. 2017, doi:10.1109/ICDCS.2017.206.

[52] X. Wang, C. Yang, and S. Mao, "TensorBeat: Tensor decomposition for monitoring multiperson breathing beats with commodity WiFi," ACM Transactions on Intelligent Systems and Technology, vol. 9, no. 1, pp. 1–27, Sept. 2017, doi:10.1145/3078855.

[53] C. Chen, Y. Han, Y. Chen, HQ. Lai, F. Zhang, B. Wang, and K.J. Ray Liu, "TR-BREATH: Time-reversal breathing rate estimation and detection," IEEE Transactions on Biomedical Engineering, vol. 65, no. 3, pp. 489-501, Apr. 2017, doi:10.1109/TBME.2017.2699422.

[54] Y. Zeng, D. Wu, J. Xiong, J. Liu, Z. Liu, and D. Qing, "MultiSense: Enabling multi-person respiration sensing with commodity WiFi," Proceedings of the ACM on Interactive, Mobile, Wearable and Ubiquitous Technologies, vol. 4, no. 3, pp. 1-29, Sept. 2020, doi:10.1145/3411816.

[55] F. Zhang, Z. Chang, J. Xiong, R. Zheng, J. Ma, K. Niu, B. Jin, and D. Zhang, "Unlocking the beamforming potential of lora for long-range multi-target respiration sensing," Proceedings of the ACM on Interactive, Mobile, Wearable and Ubiquitous Technologies, vol. 5, no. 2, pp. 1-25, Jun. 2021, doi:10.1145/3463526.

[56] H. Wan, S. Shi, W. Cao, W. Wang, and G. Chen, "RespTracker: Multi-user room-scale respiration tracking with commercial acoustic devices," IEEE Conference on Computer Communications, pp. 1-10, May. 2021, doi:10.1109/INFOCOM42981.2021.9488881.

[57] Y. Zeng, D. Wu, J. Xiong, E. Yi, R. Gao, and D. Zhang, "FarSense: Pushing the range limit of WiFi-based respiration sensing with CSI ratio of two antennas," Proceedings of the ACM on Interactive, Mobile, Wearable and Ubiquitous Technologies, vol. 3, no. 3, pp. 1-26, Sept. 2019, doi:10.1145/3351279.

[58] A.D. Droitcour, "Non-contact measurement of heart and respiration rates with a single-chip microwave doppler radar," Ph.D. Dissertation, Stanford University, 2006.

[59] A. Santra, R.V. Ulaganathan, T. Finke, A. Baheti, D. Noppeney. J.R.Wolfgang, and S. Trotta, "Short-Range Multi-Mode Continuous-Wave Radar for Vital Sign Measurement and Imaging," IEEE Radar Conference, pp. 0946-0950, Apr. 2018, doi:10.1109/RADAR.2018.8378688.

[60] X. Xu, J. Yu, Y. Chen, Y. Zhu, L. Kong, and M. Li, "Breathlistener: Fine-grained breathing monitoring in driving environments utilizing acoustic signals," Proceedings of the 17th Annual International Conference on Mobile Systems, Applications, and Services, pp. 54-66, Jun. 2019, doi:10.1145/3307334.3326074.

[61] A. Farina, "Advancements in impulse response measurements by sine sweeps," Audio engineering society convention 122. Audio Engineering Society, May. 2007, http://www.aes.org/e-lib/browse.cfm?elib=14106.

[62] Sun, C. C. , et al. "Entity Resolution Oriented Clustering Algorithm." Journal of Software, vol. 27, no. 9, pp. 2303-2319, Sep. 2016, doi: 10.13328/j.cnki.jos.005043.

Tianben Wang received the B.S. degree in computer science from Northwest A&F University, Yangling, China, M.Sc. degree and Ph.D. degree in computer science from Northwestern Polytechnical University, Xi'an, China. He is currently an Associate Professor with the College of Mechanical and Electronic Engineering in Northwest A&F

University, Yangling, China. His research interests include ubiquitous computing, contactless behavior sensing and intelligent elder assisting technology. As the leading author, he has published intensively in the top conferences/journals, including ACM UbiComp, IEEE Internet of Things Journal, IEEE TSMC-S, and ACM TIST.

Zhangben Li received the B.E. degree in The College of Mechanical and Electrical Engineering from Central South University, Hunan, China in 2019. He is currently pursuing the M.S. degree in Mechanical Engineering in Northwest A&F University, Yangling, China. His current research interest is contactless behavior sensing and DSP.

Xiantao Liu received the B.E. degree in mechanical design manufacture and Automation from Weifang University, Weifang, China. He is currently pursuing master's degree in Mechanic Engineering in Northwest A&F University, Yangling, China. His current research interests include contactless sensing and embedded system design.

Tao Gu (Senior member, IEEE) obtained his Ph.D. in Computer Science from National University of Singapore, M.Sc. in Electrical and Electronic Engineering from Nanyang Technological University, and B.Eng. in Automatic Control from Huazhong University of Science and Technology. He is currently a Professor in Department of Computing at Macquarie University, Australia. He serves as an Editor of Proc. of the ACM on Interactive, Mobile, Wearable and Ubiquitous Technologies (IMWUT), an Associate Editor of IEEE Transactions on Mobile Computing (TMC) and IEEE Internet of Things Journal (IoT-J). His research interests include Internet of Things, ubiquitous computing, mobile computing, embedded AI, wireless sensor networks, and big data analytics.

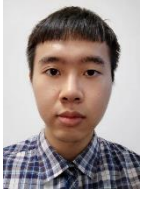

Honghao Yan received the B.E. degree in Electronic Information Engineering from Northwest A&F University, Yangling, China. He is currently pursuing master's degree in Mechanic Engineering in Northwest A&F University, Yangling, China. His current research interests include contactless sensing and machine learning.

Jing Lv received her B.E degree in computer science from Qingdao Institute of Technology, Qingdao, China and M.Sc. degree in computer science from Northwest A&F University, Yangling, China. She is currently serving as a network security engineer with the department of Network & Education Technology Center, Northwest A&F University, Yangling 712100, China.

Jin Hu received the Ph.D degree from Northwest A & F University, Yangling, China in 2016. She is currently an Associate Professor with the Northwest A & F University, Yangling, China. Her research interest includes agricultural internet of things technology and agricultural information intelligent decision-making.

Daqing Zhang (Fellow, IEEE) received the Ph.D. degree from the University of Rome "La Sapienza", Italy, in 1996. He is a Chair Professor with the Department of Computer Science and Technology, Peking University, China, and Telecom SudParis, France. His current research interests include context aware computing, urban computing, mobile computing, big data analytics, and pervasive elderly care. He has published over 280 technical papers in leading conferences and journals.

Professor hang was a recipient of the Ten-Years CoMoRea Impact Paper Award at IEEE PerCom2013, the Honorable Mention Award at ACM UbiComp 2015 and 2016, the Best Paper Award at IEEE UIC 2012 and 2015. He served as the General or Program Chair for over 17international conferences, giving keynote talks at more than 20 international conferences. He is an Associate Editor for IEEE Pervasive Computing, ACM Transactions on Intelligent Systems and Technology, and Proceedings of the ACM on Interactive, Mobile, Wearable and Ubiquitous Technologies.